# BOSE-EINSTEIN FINAL STATE SYMMETRIZATION FOR EVENT GENERATORS OF HEAVY ION COLLISIONS

U.A. Wiedemann[a,b], J. Ellis[c], U. Heinz[a] and K. Geiger[d]
[a] *Institut für Theoretische Physik, Universität Regensburg, D-93040 Regensburg*
[b] *Physics Department, Columbia University, New York, N.Y. 10027, U.S.A.*
[c] *Theoretical Physics Division, CERN, CH-1211 Geneva 23*
[d] *Physics Department, BNL, Upton, N.Y. 11973, U.S.A.*

We discuss algorithms which allow to calculate identical two-particle correlations from numerical simulations of relativistic heavy ion collisions. A toy model is used to illustrate their properties.

## 1 Introduction

The current relativistic heavy ion program at CERN and BNL aims at investigating the equilibration properties of hadronic matter at extreme temperatures and densities where quarks and gluons are expected to be the physically relevant degrees of freedom for particle production processes. The theoretical discussion of these collision systems is complicated by their mesoscopic character. They are not sufficiently small to allow for an analytical description in terms of elementary processes. They are not sufficiently large to take a description in terms of macroscopic observables for granted. Even if simple thermodynamically or hydrodynamically inspired models account for the data, the task remains to understand the microscopic origin of their success, and to establish to what extent such an agreement is necessary or accidental.

Numerical simulations of relativistic heavy ion collisions are an adequate tool to attack these questions. They allow to propagate sufficiently many degrees of freedom from some initial condition, and they thus test the consequences of different assumptions about the microscopic in medium dynamics. Many event generators have been developed to this aim [1]. Irrespective of their particular model assumptions, they return for each simulated event a set of $N_m$ phase space emission points $\{(\check{\mathbf{r}}_i, \check{\mathbf{p}}_i, \check{t}_i)\}_{i\in[1,N_m]}$ together with information, e.g., about the identity (PID) of the particle $i$, the parent resonance it originates from, the number of rescatterings it has undergone, etc.

The major aim of event generator studies is to reduce step by step the class(es) of dynamical scenarios consistent with experimental data, thus obtaining an increasingly better picture of the physics. To this end, one mainly compares the simulated particle ratios and one-particle momentum spectra to experiment. However, one can imagine different dynamical scenarios which all

account for the same simulated momentum distributions $\{(\check{\mathbf{p}}_i)\}_{i\in[1,N_m]}$ but differ with respect to the simulated space-time structure $\{(\check{\mathbf{r}}_i,\check{t}_i)\}_{i\in[1,N_m]}$. Identical two-particle correlations $C(\mathbf{q},\mathbf{K})$, here written as a function of the measured pair momentum $K=\frac{1}{2}(p_1+p_2)$ and relative pair momentum $q=p_1-p_2$ are sensitive to the latter and can thus play an important complementary role in specifying the parameter space of event generators. Here, we discuss algorithms of the type

$$\left\{\{(\check{\mathbf{r}}_i,\check{\mathbf{p}}_i,\check{t}_i)\}_{i\in[1,N_m]}\right\}_{m\in[1,N_{\rm ev}]} \Longrightarrow C(\mathbf{q},\mathbf{K})\,. \tag{1}$$

For notational convenience, we restrict the following discussion to one particle species only, like-sign pions say. Also, we neglect final state Coulomb and strong interactions [2]. The set $\{(\check{\mathbf{r}}_i,\check{\mathbf{p}}_i,\check{t}_i)\}_{i\in[1,N_m]}$ denotes then the phase space emission points of the $N_m$ like-sign pions generated in the $m$-th simulated event. The event generator simulates thus a classical phase space distribution

$$\rho_{\rm class}(\mathbf{r},\mathbf{p},t)=\frac{1}{N_{\rm ev}}\sum_{m=1}^{N_{\rm ev}}\sum_{i=1}^{N_m}\delta^{(3)}(\mathbf{r}-\check{\mathbf{r}}_i)\,\delta^{(3)}(\mathbf{p}-\check{\mathbf{p}}_i)\,\delta(t-\check{t}_i)\,. \tag{2}$$

## 2 From phase space densities to momentum correlations

The standard particle interferometric analysis of heavy ion collisions starts from the relation between the measured momentum correlations of identical particles and the quantum mechanical Wigner phase space density $S(x,K)$ of particle emitting sources in the collision region [3],

$$C(\mathbf{q},\mathbf{K})=\mathcal{N}\left(1+\frac{\left|\int d^4x\,S(x,K)\,e^{iq\cdot x}\right|^2}{\int d^4x\,S(x,p_1)\;\int d^4y\,S(y,p_2)}\right)\,. \tag{3}$$

This expression can be generalized to include final state interactions [2]. Depending on the definition of the two-particle correlator in terms of single- and two-particle cross sections [4,5] (respectively depending on its construction from experimental data), the normalization is either $\mathcal{N}=1$ or $\mathcal{N}<1$. The calculation of deviations of $\mathcal{N}$ from 1 typically involves multiparticle symmetrization effects [6,5], which we do not review here. Our discussion will thus be for $\mathcal{N}=1$.

In the light of Eq. (3), calculating the two-particle correlator $C(\mathbf{q},\mathbf{K})$ from an event generator output amounts to specifying the emission function $S(x,K)$ in terms of the generated phase space points $\{(\check{\mathbf{r}}_i,\check{\mathbf{p}}_i,\check{t}_i)\}_{i\in[1,N_m]}$, i.e., it amounts to an interpretation of $(\check{\mathbf{r}}_i,\check{\mathbf{p}}_i,\check{t}_i)$. In sections 2.1 and 2.2, we focus on

two different interpretations referred to as *quantum mechanical* and *classical*, though they are both conceptually on an equal footing. Before doing that, we list here three requirements which an algorithm implementing (1) should fulfill:

1. Event generators use *probabilities* to describe the collision process. Bose-Einstein correlations are obtained from squaring production *amplitudes*. Hence, the generated momenta $\check{\mathbf{p}}_i$, $\check{\mathbf{p}}_j$ do not show the enhancement at low relative momenta characteristic for Bose-Einstein final state symmetrization. The prescriptions (1) should calculate this effect a posteriori.

2. The strength of Bose-Einstein correlations depends on the distance of the identical particles in phase space, not in momentum space. We thus require the prescriptions (1) to use the entire phase space information, and not only the generated momentum information. 'Weighting' or 'shifting' prescriptions which are based only on the latter may successfully match the measured momentum correlations but obviously do not allow to test the simulated space-time structure.

3. In general, Bose-Einstein statistics can affect particle multiplicity distributions during the particle production process. However, event generators are tuned to reproduce the average particle multiplicities in agreement with the data. We require hence that the prescriptions (1) conserve particle multiplicities. If the correlator is interpreted as a factor, relating measured two-particle differential cross sections to those simulated by the event generator, $d^6\sigma_{\rm meas}/d^3\mathbf{p}_1\, d^3\mathbf{p}_2 = C(\mathbf{q},\mathbf{K})\; d^6\sigma_{\rm sim}/d^3\mathbf{p}_1\, d^3\mathbf{p}_2$, then this implies [11,6] that $\mathcal{N} < 1$ in (3). This however plays no role in what follows since the space-time analysis of correlation data can be based entirely on the momentum dependence of $C(\mathbf{q},\mathbf{K})$, disregarding its absolute normalization.

### *2.1 "Quantum" interpretation of event generator output*

In the *quantum mechanical* interpretation [8,9,6,10], the set of phase space points $\{\{(\check{\mathbf{r}}_i, \check{\mathbf{p}}_i, \check{t}_i)\}_{i\in[1,N_m]}\}_{m\in[1,N_{\rm ev}]}$ is associated to the centers of Gaussian one-particle wavepackets according to [7,8,9]

$$(\check{\mathbf{p}}_i, \check{\mathbf{r}}_i, \check{t}_i) \longrightarrow f_i(\mathbf{x}, \check{t}_i) = \frac{1}{(\pi\sigma^2)^{3/4}} \mathrm{e}^{-\frac{1}{2\sigma^2}\,(\mathbf{x}-\check{\mathbf{r}}_i)^2 \,+\, i\check{\mathbf{p}}_i\cdot\mathbf{x}}\,. \tag{4}$$

These wavepackets $f_i$ are quantum mechanically best localized states, i.e., they saturate the Heisenberg uncertainty relation with $\Delta x_i = \sigma/\sqrt{2}$ and $\Delta p_i =$

$1/\sqrt{2}\sigma$.

Taking only two-particle symmetrized contributions into account, i.e., adopting the so-called pair approximation, all spectra can be written in terms of the functions $s_i(\mathbf{p})$, which coincide with the corresponding one-particle spectrum for a source emitting only one particle at the phase space point $i$. For the one- and two-particle correlator one finds [9,8]

$$E_p \frac{d^3N}{d^3p} = \frac{1}{N_{\rm ev}} \sum_{m=1}^{N_{\rm ev}} \nu_m(\mathbf{p}) = \frac{1}{N_{\rm ev}} \sum_{m=1}^{N_{\rm ev}} \sum_{i=1}^{N_m} s_i(\mathbf{p})\,, \tag{5}$$

$$C(\mathbf{q},\mathbf{K}) = 1 + e^{-\sigma^2\mathbf{q}^2/2} \frac{\sum_{m=1}^{N_{\rm ev}} \left[ \left| \sum_{i=1}^{N_m} s_i(\mathbf{K})\, e^{iq^0\check{t}_i - i\mathbf{q}\cdot\check{\mathbf{r}}_i} \right|^2 - \sum_{i=1}^{N_m} s_i^2(\mathbf{K}) \right]}{\sum_{m=1}^{N_{\rm ev}} \left[ \nu_m(\mathbf{p}_a)\,\nu_m(\mathbf{p}_b) - \sum_{i=1}^{N_m} s_i(\mathbf{p}_a)\, s_i(\mathbf{p}_b) \right]} \tag{6}$$

$$s_i(\mathbf{p}) = \pi^{-3/2}\,\sigma^3\, e^{-\sigma^2(\mathbf{p}-\check{\mathbf{p}}_i)^2}\,. \tag{7}$$

Here, the terms subtracted in the numerator and denominator of $C(\mathbf{q},\mathbf{K})$ are finite multiplicity corrections which become negligible for large particle multiplicities [8]. This algorithm is consistent with an emission function $S(x,\mathbf{K})$

$$S(x,\mathbf{K}) = \int d\check{\mathbf{r}}_i\, d\check{\mathbf{p}}_i\, d\check{t}_i\, \rho_{\rm class}(\check{\mathbf{r}}_i,\check{\mathbf{p}}_i,\check{t}_i)\, s_0(\mathbf{x}-\check{\mathbf{r}}_i, t-\check{t}_i, \mathbf{K}-\check{\mathbf{p}}_i)\,, \tag{8}$$

$$s_0(x,\mathbf{K}) = \tfrac{1}{\pi^3}\,\delta(t)\,\mathrm{e}^{-\frac{1}{\sigma^2}\mathbf{x}^2 - \sigma^2\mathbf{K}^2}\,, \tag{9}$$

which is given by a folding relation between a classical distribution $\rho_{\rm class}$ of wavepacket centers and the elementary source Wigner function $s_0(x,\mathbf{K})$. The latter has at emission an optimal quantum mechanical phase space localization around phase space points $(\check{\mathbf{r}}_i,\check{\mathbf{p}}_i,\check{t}_i)$ with spatial uncertainty $\sigma$ and momentum uncertainty $1/\sigma$.

In the algorithm (5)-(7), the spectra are discrete functions of the input $(\check{\mathbf{r}}_i,\check{\mathbf{p}}_i,\check{t}_i)$ but they are continuous in the observable momenta $\mathbf{p}_1$, $\mathbf{p}_2$ and hence, no binning is necessary. Also, the number of terms to be calculated in (5) and (6) grows linear in $N$, not quadratic as in other prescriptions. However, both the one- and two-particle spectra depend in this algorithm on the wavepacket width $\sigma$. The role of this parameter will be discussed in the context of our toy model study in section 3.

### *2.2 "Classical" interpretation of event generator output*

In the *classical* interpretation [9,10], the phase space points $(\check{\mathbf{r}}_i,\check{\mathbf{p}}_i,\check{t}_i)$ are seen as a discrete approximation of the on-shell Wigner phase space density $S(x,p)$,

$$S(x,\mathbf{p}) = \rho_{\rm class}(\mathbf{x},\mathbf{p},t)\,. \tag{10}$$

This defines both the two-particle correlator via (3) and the one-particle spectrum via the $x$-integration over (10). To simplify a numerical implementation of this calculation, it is useful to replace the $\delta$ functions of $\rho_{\rm class}$ in momentum space by rectangular 'bin functions' [9], or by properly normalized Gaussians [10] of width $\epsilon$,

$$\delta^{(\epsilon)}_{\check{\mathbf{p}}_i,\mathbf{p}} = \frac{1}{(\pi\epsilon^2)^{3/2}} \exp\left(-(\check{\mathbf{p}}_i - \mathbf{p})^2/\epsilon^2\right) . \tag{11}$$

In the limit $\epsilon \to 0$, these Gaussian bin functions reduce to the properly normalized $\delta$-functions $\delta^{(3)}(\check{\mathbf{p}}_i - \mathbf{p})$ and we regain Eq. (2). The one-particle spectrum and two-particle correlator read then [9,10]

$$E_p \frac{d^3N}{d^3p} = \int d^4x\, S(x,\mathbf{p}) = \frac{1}{N_{\rm ev}} \sum_{m=1}^{N_{\rm ev}} \sum_{i=1}^{N_m} \delta^{(\epsilon)}_{\check{\mathbf{p}}_i,\mathbf{p}} \,, \tag{12}$$

$$C(\mathbf{q},\mathbf{K}) = 1 + \frac{\sum_{m=1}^{N_{\rm ev}} \left[ \left| \sum_{i=1}^{N_m} \delta^{(\epsilon)}_{\check{\mathbf{p}}_i,\mathbf{K}}\, e^{iq^0\check{t}_i - i\mathbf{q}\cdot\check{\mathbf{r}}_i} \right|^2 - \sum_{i=1}^{N_m} \left(\delta^{(\epsilon)}_{\check{\mathbf{p}}_i,\mathbf{K}}\right)^2 \right]}{\sum_{m=1}^{N_{\rm ev}} \left[ \left(\sum_{i=1}^{N_m} \delta^{(\epsilon)}_{\check{\mathbf{p}}_i,\mathbf{p}_1}\right) \left(\sum_{j=1}^{N_m} \delta^{(\epsilon)}_{\check{\mathbf{p}}_j,\mathbf{p}_2}\right) - \sum_{i=1}^{N_m} \delta^{(\epsilon)}_{\check{\mathbf{p}}_i,\mathbf{p}_1} \delta^{(\epsilon)}_{\check{\mathbf{p}}_i,\mathbf{p}_2} \right]} . \tag{13}$$

The correlator (13) is the discretized version of the Fourier integrals in (3). The subtracted terms in the numerator and denominator remove discretization errors which would amount to pairs constructed from the same particles. The 'classical' algorithm has the same important advantages as the 'quantum' one, it involves only $O(N_m)$ rather than $O(N_m^2)$ numerical manipulations per event, and its observables are discrete functions of the input, but continuous functions of the measured momenta; hence, no binning is necessary. 'Classical' and 'quantum' algorithm then differ only with respect to two points:

1. The classical algorithm has no analogue for the Gaussian prefactor $\exp\left(-\sigma^2\,\mathbf{q}^2/2\right)$ in (6) which is a genuine quantum effect stemming from the quantum mechanical localization properties of (4).

2. For the choice $\sigma = 1/\epsilon$, the bin functions $\delta^{(\epsilon)}_{\check{\mathbf{p}}_i,\mathbf{p}}$ is the classical counterpart of the Gaussian single-particle distributions $s_i(\mathbf{p})$. Finite event statistics puts a lower practical limit on $\epsilon$, but the physical momentum spectra are recovered in the limit $\epsilon \to 0$, i.e., $\epsilon$ should be chosen as small as technically possible. In contrast, the quantum algorithm treats $\sigma$ as finite physical localization of the single particle wavepackets. The limit $\sigma \to \infty$ (which corresponds to $\epsilon \to 0$) is not the physically relevant case. It amounts according to (8) to an emission function which is infinitely extended in space, and hence [8] $\lim_{\sigma\to\infty} C(\mathbf{q},\mathbf{K}) = 1 + \delta_{\mathbf{q},0}$.

## 3 The Zajc model

Our final aim is to apply the above algorithms to event generators of relativistic heavy ion collisions and high energy elementary processes. A first step in this direction will be reported in [10]. Here, we illustrate the properties of these algorithms for a toy model.

The strategy is to start from a simple expression for the classical distribution $\rho_{\rm class}$, from which the results of the algorithms of sections 2.1 and 2.2 can be calculated analytically. In a second step, we generate then in a Monte Carlo procedure sets of phase space points $\{(\check{\mathbf{r}}_i, \check{\mathbf{p}}_i, \check{t}_i)\}_{i\in[1,N_m]}$ according to this distribution, and we test the numerical results against our exact analytical expressions. This allows us to make in an analytically controlled setting statements about i) the $\sigma$-dependence of the quantum algorithm, ii) the $\epsilon$-dependence of the classical algorithm (especially: how small $\epsilon$ has to be chosen to extract the limit $\epsilon \to 0$ numerically) and iii) the statistical requirements for the algorithms to work.

Here, we study these questions for the Zajc model which describes a position-momentum correlated phase space distribution of emission points [12]

$$\rho^{\rm Zajc}_{\rm class}(\mathbf{r},\mathbf{p},t) = \mathcal{N}_s \, \exp\left\{-\frac{1}{2(1-s^2)}\left(\frac{\mathbf{r}^2}{R_0^2} - 2s\frac{\mathbf{r}\cdot\mathbf{p}}{R_0 P_0} + \frac{\mathbf{p}^2}{P_0^2}\right)\right\}\delta(t)\,, \quad (14)$$

$$\mathcal{N}_s = E_p\,\frac{N}{(2\pi)^3\,R_0^3\,P_0^3\,(1-s^2)^{3/2}}\,. \quad (15)$$

This distribution is normalized such that the total event multiplicity calculated from the one-particle spectrum (12) is $N$. The parameter $s$ smoothly interpolates between completely uncorrelated and completely position-momentum correlated sources. For $s \to 0$, the position-momentum correlation vanishes and we are left with the product of two Gaussians in position and momentum space. In the opposite limit

$$\lim_{s\to 1} \rho^{\rm Zajc}_{\rm class}(\mathbf{r},\mathbf{p},t) \sim \delta^{(3)}\left(\frac{\mathbf{r}}{R_0} - \frac{\mathbf{p}}{P_0}\right)\,\delta(t)\,, \quad (16)$$

the position-momentum correlation is perfect. The corresponding phase space volume of the distribution is proportional to

$$V = 2^3\,R_0^3\,P_0^3\,(1-s^2)^{3/2}\,, \quad (17)$$

and goes to zero for $s \to 1$. This strong $s$-dependence allows to study the performance of our numerical algorithms for different phase space volumes. In the following subsections, we discuss the $s$-dependence of the one-particle spectrum and two-particle correlator, focussing in sections 3.1 and 3.2 on analytical results, and comparing these in section 3.3 to numerical calculations.

### *3.1 The Zajc model in the classical algorithm*

Starting from an analytical emission function $S(x,\mathbf{p}) = \rho_{\rm class}(\mathbf{x},\mathbf{p},t)$ according to (10), the one-particle spectrum and two-particle correlator read

$$E_p \frac{dN}{d^3p} = E_p \frac{N}{(2\pi)^{3/2} P_0^3} \exp\left(-\frac{\mathbf{p}^2}{2P_0^2}\right) , \tag{18}$$

$$C(\mathbf{q},\mathbf{K}) = 1 + \exp\Big(-\mathbf{q}^2 R^2_{\rm class}(\epsilon)\Big) , \tag{19}$$

$$R^2_{\rm class}(\epsilon) = R_0^2 \left(1 - s^2 \frac{1}{1+\epsilon^2/2P_0^2} - \frac{1}{(2P_0R_0)^2} \frac{1}{1+\epsilon^2/2P_0^2}\right) . \tag{20}$$

We recover the physical HBT radius from (20) in the limit $\epsilon \to 0$ or by inserting (10) directly into (2). The remarkable fact is that for sufficiently large $s$ [12],

$$s > s_{\rm crit} = \sqrt{1 - \frac{1}{(2R_0P_0)^2}} , \tag{21}$$

the HBT radius $R^2_{\rm class}$ becomes negative and the two-particle correlator shows an unphysical rise of the correlation function with increasing $\mathbf{q}^2$. The change of sign in (19) seems to be related to the violation of the uncertainty relation by the emission function (14): In the limiting case (16), $\rho^{\rm Zajc}_{\rm class}$ reduces to a perfect position-momentum correlated source which is not consistent with the Heisenberg uncertainty relation. Also, the phase space volume $V$ in (17) drops below 1 for $s > s_{\rm crit}$. In this sense, the distribution $\rho^{\rm Zajc}_{\rm class}$ is a quantum mechanically allowed emission function $S(x,\mathbf{p}) = \rho_{\rm class}(\mathbf{x},\mathbf{p},t)$ for $s < s_{\rm crit}$ only.

Clearly, an ansatz for a quantum mechanical Wigner phase space density $S(x,K)$ has to satisfy quantum mechanical localization properties. However, realistic event generators satisfy this requirement anyway. The practical importance of (this limiting case of) the Zajc model is thus that it provides an (extreme) testing ground for our numerical algorithms. Analytically, we conclude already from (20) that a bin width sufficient to investigate the limit $\epsilon \to 0$, has to be small on the scale of the width of the generated momentum distribution,

$$\epsilon \ll \sqrt{2}\, P_0 . \tag{22}$$

At least for the present model study, this requirement is independent of the strength of position-momentum correlations in the source.

### *3.2 The Zajc model in the quantum algorithm*

We now interprete the classical probability distribution $\rho^{\rm Zajc}_{\rm class}$ of (14) as a distribution of phase space points associated with the centers of Gaussian wavepack-

ets according to (4). The one-particle spectrum and two-particle correlator are then readily calculated via the emission function (8),

$$E_p \frac{dN}{d^3p} = E_p \frac{N}{(2\pi)^{3/2}(P_0^2 + 1/2\sigma^2)^{3/2}} \exp\left(-\frac{\mathbf{p}^2}{2P_0^2 + 1/\sigma^2}\right), \tag{23}$$

$$C(\mathbf{q}, \mathbf{K}) = 1 + \exp\Big(-\mathbf{q}^2 R_{\rm qm}^2\Big), \tag{24}$$

$$R_{\rm qm}^2 = \frac{\sigma^2}{1 + 2\sigma^2 P_0^2}\left(\sigma^2 P_0^2 + R_0^2/\sigma^2 + 2R_0^2 P_0^2(1 - s^2)\right). \tag{25}$$

In contrast to the classical algorithm, the radius parameter is now always positive, irrespective of the value of $s$. Even if the classical distribution $\rho_{\rm class}^{\rm Zajc}(\check{\mathbf{r}}, \check{\mathbf{p}}, \check{t})$ is sharply localized in phase space, its folding with minimum uncertainty wave packets leads to a quantum mechanically allowed emission function $S(x, \mathbf{p})$ and to a correlator with falls off with increasing $\mathbf{q}^2$ as expected. However, the spread of the one-particle momentum spectrum (23) receives an additional contribution $1/\sigma^2$. Choosing $\sigma$ too small increases this term beyond the phenomenologically reasonable values, choosing it too large widens the corresponding HBT radius parameters significantly. It was argued[8] that $\sigma$ can be interpreted as quantum mechanical 'size' of the particle, $\sigma \approx 1$ fm. Given the heuristic nature of these arguments and the significant modifications this implies for the spectra (23) and (24), it is however fair to say that presently $\sigma$ mainly plays the role of a regulator of unwanted violations of the quantum mechanical uncertainty principle while a deeper understanding of its origin in the particle production dynamics is still missing.

### *3.3 Numerical simulation in the Zajc model*

We have studied the performance of our Bose-Einstein algorithms by generating with a random number generator sets $\{(\check{\mathbf{r}}_i, \check{\mathbf{p}}_i, \check{t}_i)\}_{i\in[1,N_m]}$ of phase space points according to the distribution $\rho_{\rm class}^{\rm Zajc}$ and comparing the numerical results of our algorithms to the analytical expressions of section 3.1 and 3.2.

In Fig. 1(a), the $\epsilon$-dependence of the HBT-radius parameter (20) is depicted. For fixed bin width $\epsilon$, the approximation of the true HBT radius parameter by $R_{\rm class}^2(\epsilon)$ is seen to become better with increasing $P_0$, in agreement with (22). For the HBT radius obtained from the quantum version of the Zajc model and depicted in Fig. 1(b), the situation is both qualitatively and quantitatively different. Now, the HBT radius is always positive, since the Gaussian wavepackets take quantum mechanical localization properties automatically into account. Also, the $s$-dependence of the radius is seen to be much smaller, since the wavepackets smear out the unphysically strong position-momentum

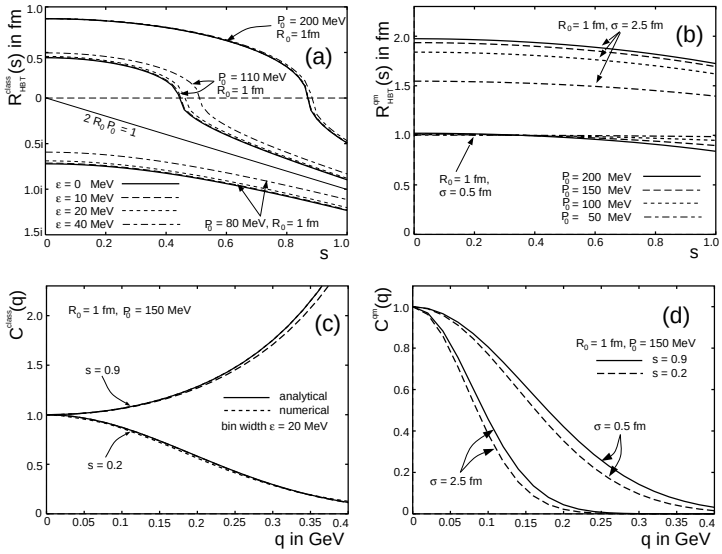


Figure 1: Generic properties of the one-dimensional Zajc model. (a) HBT-radius parameter (20) of the classical interpretation as a function of the position momentum correlation $s$. The plot shows the HBT radius for different combinations of the model-parameters $R_0$ and $P_0$, and for different sizes of the bin width $\epsilon$ needed in numerical implementations. (b) same as (a) for the quantum version of the model, eq. (25). The dependence of the HBT radius on the wavepacket width $\sigma$ is seen clearly. (c) and (d) The two-particle correlator in the classical (c) and quantum mechanical (d) version of the model for different sets of model parameters. The numerical results are obtained for 50 events of multiplicity 1000, and agree very well with the analytical calculations.

correlations present in the classical distribution $\rho^{\rm Zajc}_{\rm class}$. The HBT radius depends not only on the geometrical size $R_0$, and on the momentum width $P_0$ of the source, but also on the wavepacket width $\sigma$. As seen in Fig. 1(b), this wavepacket width affects the HBT radius and its $P_0$-dependence significantly for $\sigma > R_0$.

In Fig. 1(c) and (d) we have presented the two-particle correlation functions corresponding to these HBT-radius parameters for characteristic values of the model parameters. The analytical results, obtained by plotting (19) and (24) are compared to the results of an application of the event generator algorithms (6) and (13) for a Monte Carlo phase space distribution $\rho^{\rm Zajc}_{\rm class}$ of phase space points. The present plot is obtained for 50 events of multiplicity 1000. The differences between analytical and numerical results have their origin in statistical fluctuations and become smaller with increasing number of events

$N_{\rm ev}$ or event multiplicity $N_m$. The good agreement between analytical and numerical results in Fig. 1(c,d) indicates the relatively low statistical requirements of our algorithms. The reason is that both algorithms associate to the *discrete* set of generated momenta $\check{\mathbf{p}}_i$ *continuous* functions of the measured momenta $\mathbf{p}_1$, $\mathbf{p}_2$. This smoothens any statistical fluctuation significantly. For the classical algorithm, small deviations between numerical and analytical results are still visible in Fig. 1(c), while the results of the quantum algorithm coincide within line width. This can be traced back to the Gaussian prefactor $\exp\left(-\sigma^2\,\mathbf{q}^2/2\right)$ in eq. (6) which provides an additional smoothening of statistical fluctuations not present in the classical algorithm.

**Acknowledgments**

This is a report on work in progress. The presenting author, U.A.W., would like to acknowledge a DFG-Habilitationsstipendium. He also thanks the CRIS'98 Local Organizing Comittee for generous support which made his participation at this Conference possible.

**References**

1. Y. Pang, Talk at the 13th Intl. Conf. on Ultra-Relativistic Nucleus-Nucleus Collisions (Quark Matter'97), Nucl. Phys. **A** to be published.
2. D.V. Anchishkin, U. Heinz and P. Renk, Phys.Rev. C57 (1998) 1428.
3. U. Heinz, in: *Correlations and Clustering Phenomena in Subatomic Physics*, ed. by M.N. Harakeh, O. Scholten, and J.H. Koch, NATO ASI Series (Plenum, New York, 1996), p. 137.
4. D. Miśkowiec and S. Voloshin, nucl-ex/9704006.
5. Q.H. Zhang, P. Scotto and U. Heinz, nucl-th/9805046.
6. U.A. Wiedemann, Phys. Rev. **C57** (1998) 3324.
7. H. Merlitz and D. Pelte, Z. Phys. **A357**, 175 (1997).
8. U.A. Wiedemann, P. Foka, H. Kalechofsky, M. Martin, C. Slotta and Q.H. Zhang, Phys. Rev. C**56**, R614 (1997).
9. Q.H. Zhang, U.A. Wiedemann, C. Slotta and U. Heinz, Phys. Lett. **B**407, 33 (1997).
10. J. Ellis, K. Geiger, U. Heinz and U.A. Wiedemann, in preparation.
11. L. Lönnblad and T. Sjöstrand, Phys. Lett. **B351**, 293 (1995); Eur.Phys.J. C2 (1998) 165-180
12. W.A. Zajc, Particle Production in Highly Matter, ed. H.H. Gutbrod and J. Rafelski, NATO ASI Series B303 (Plenum Press, New York), 1993, p. 435.